Angular distribution of elastic scattering induced by ^{17}F on medium-mass target nuclei at energies near the Coulomb barrier

G. L. Zhang,[1,2,*] G. X. Zhang,[1] C. J. Lin,[3,8,†] J. Lubian,[4] J. Rangel,[4] B. Paes,[4] J. L. Ferreira,[4] H. Q. Zhang,[3] W. W. Qu,[1,6] H. M. Jia,[3] L. Yang,[3] N. R. Ma,[3] L. J. Sun,[3] D. X. Wang,[3] L. Zheng,[1] X. X. Liu,[1] X. T. Chu,[1] J. C. Yang,[1] J. S. Wang,[5] S. W. Xu,[5] P. Ma,[5] J. B. Ma,[5] S. L. Jin,[5] Z. Bai,[5] M. R. Huang,[5] H. L. Zang,[7] B. Yang,[7] and Y. Liu[7]

[1]*School of Physics and Nuclear Energy Engineering, Beihang University, Beijing 100191, China*
[2]*Beijing Advanced Innovation Center for Big Data-Based Precision Medicine, Beihang University, Beijing 100083, China*
[3]*China Institute of Atomic Energy, Beijing 102413, China*
[4]*Instituto de Física, Universidade Federal Fluminense, Avenida Litoranea s/n, Gragoatá, Niterói, Rio de Janeiro 24210-340, Brazil*
[5]*CAS Key Laboratory of High Precision Nuclear Spectroscopy, Institute of Modern Physics, Chinese Academy of Sciences, Lanzhou 730000, China*
[6]*School of Radiation Medicine and Protection, Medical College of Soochow University, Soochow 215123, China*
[7]*School of Physics and State Key Laboratory of Nuclear Physics and Technology, Peking University, Beijing 100871, China*
[8]*College of Physics and Technology, Guangxi Normal University, Guilin 541004, China*

The elastic scattering angular distributions were measured for 50- and 59-MeV ^{17}F radioactive ion beam on a ^{89}Y target. The aim of this work is to study the effect of the breakup of the proton halo projectile on the elastic scattering angular distribution. The experimental data were analyzed by means of the optical model with the double-folding São Paulo potential for both real and imaginary parts. The theoretical calculations reproduced the experimental data reasonably well. It is shown that the method of the data analysis is correct. In order to clarify the difference observed at large angles for the 59-MeV incident energy data, Continuum-Discretized Coupled-Channels (CDCC) calculations were performed to consider the breakup coupling effect. It is found that the experimental data show the Coulomb rainbow peak and that the effect of the coupling to the continuum states is not very significant, producing only a small hindrance of the Coulomb rainbow peak and a very small enhancement of the elastic scattering angular distribution at backward angles, suggesting that the multipole response of the neutron halo projectiles is stronger than that of the proton halo systems.

I. INTRODUCTION

The nuclear reaction dynamics induced by the nuclei near or at the drip line is one of the main research topics of current interest. In particular, light nuclei located near the drip line may exhibit an exotic nuclear structure, such as halo-skin structure. At low energies, close to the Coulomb barrier, the reaction dynamics is mainly dominated by fusion and direct processes such as elastic and inelastic scatterings, breakup, and transfer [1–6]. In the past three decades, the development of radioactive ion beams (RIBs) has intensified this kind of study. For the exotic nuclei, the basic question is whether fusion is enhanced owing to the large extent of nuclear matter distribution or hindered due to the very low breakup threshold. For the ^{6}He + ^{209}Bi [7,8] and ^{8}B + ^{58}Ni [9] systems, the fusion cross sections at energies near and below the barrier are enhanced with respect to normal systems. The fusion cross section of the ^{17}F + ^{208}Pb system was measured at energies near and below the Coulomb barrier [10] and no enhancement was observed. This may reflect the fact that the breakup cross section is too weak to influence the fusion probability. Other important reaction channels, like transfers or collective excitations, were also found not to be relevant for this system in this energy region. Although the ^{17}F isotope is a proton-rich nucleus, it has a halo structure only in its first excited state, while other proton-rich nuclei (like ^{8}B) or neutron-rich nuclei (like ^{6,8}He, ^{11}Li, and ^{11}Be) have halo or Borromean structures already in their ground state.

Experimental efforts have been made to study the influence of breakup of halo projectiles on the subbarrier fusion [11,12]. However, the data and the studies on breakup effects on the fusion cross section are still quite scarce and with very large error bars, especially at energies below the Coulomb barrier. Most of the experimental data measured for the systems involving halo projectiles concerns the effect of breakup on the elastic scattering angular distribution. The main reason is that the elastic scattering is one of the most intense channels and for this reason is easier to measure. Another reason is the possibility to immediately observe the dynamics and statics effects of the breakup channels on elastic scattering distribution. It is well known that for heavy-ion collisions, at near Coulomb-barrier energies, the elastic scattering angular distribution normalized by Rutherford shows some oscillations around one at forwards angles, passing through a peak and then

*zgl@buaa.edu.cn
†cjlin@ciae.ac.cn

starting to fall down as the angle increases. This is a result of two effects: the rainbow scattering produced by the real part of the interaction and Fresnel diffraction effects originated by both the Coulomb repulsion plus strong nuclear absorption. It is important to study if this common behavior of the heavy-ion elastic scattering remains in the case of the reaction involving proton halo projectiles. The present research is intended to explore breakup effect of the ^{17}F proton halo projectile on its elastic scattering by a medium mass target at energies around Coulomb barrier.

From the optical-model analysis of the elastic scattering at energies near the Coulomb barrier, the total reaction cross sections can be derived and the breakup effects on other channels may be examined. Information about the nuclear potential of the interacting nuclei can also be extracted from the angular distribution of the elastic scattering. While the energy dependence of the optical potential for reactions induced by tightly bound nuclei shows the well-known threshold anomaly [13,14], most of the ones for reactions induced by weakly bound nuclei shows the so-called breakup threshold anomaly [15]. As a result, studies of elastic scattering induced by light loosely bound exotic nuclei are of particular interest. Many experiments and theoretical studies of the elastic scattering for exotic nuclei have been done (see, for example, Ref. [1] and references therein). However, the data of elastic scattering for light exotic nuclei are still very scarce, which influences directly the accuracy and reliability of nuclear structure information extracted from the reaction studies. In addition, the loosely bound radioactive projectiles tend to be easily broken up during their collisions with the target through the excitation of the core-valence nuclear system to continuum states. As a result, in the extraction of the optical potential, the couplings of the breakup and/or transfer channels with the elastic channel should be carefully considered. Recently, several studies used elastic scattering to explore dynamic, static, and geometric effects of exotic projectiles [16–19]. However, systematic behaviors of this kind of nuclei are still not clear. This field needs to be further explored.

The main goal of the present work is to study the ^{17}F elastic scattering at energies close to the Coulomb barrier. ^{17}F is a proton-rich nucleus located near the proton drip line with 601-keV binding energy of its valence proton. Its first excited state ($E_x = 495$ keV, $J^\pi = 1/2^+$) is the only bound state below the breakup threshold and has a proton halo structure [20,21]. Many experiments with ^{17}F as a projectile have been done in recent years [10,22–29]. The elastic scattering of ^{17}F was primarily explored on the heavy target ^{208}Pb [25–27], where the Coulomb breakup is expected to be dominant, and then on light target ^{12}C [28,29], where nuclear interactions are expected to prevail. Except for the data of ^{17}F on ^{58}Ni [30], the experimental data about ^{17}F elastic scattering on medium-mass targets are completely missing. For medium-mass target, a strong nuclear-Coulomb interference is expected, as it was observed in the interaction of the ^{8}B proton halo projectile with the same target [31,32]. Thus, it is important to explore the elastic scattering of ^{17}F on medium-mass targets. For ^{17}F on ^{58}Ni experiment, only two energies were measured [30] and these two energies were very close. For this reason, it was not possible to determine whether the reduced total reaction cross

sections are enhanced or hindered at energies near Coulomb barrier. So, the lower energy part of the excitation function needs to be studied.

In a more recent experiment, the elastic scattering angular distribution of the system involving a neutron halo projectile, the ^{11}Be + ^{64}Zn system, was compared with the angular distribution of other two systems involving the weakly bound ^{9}Be and the stable ^{10}Be on the same target, at energies around the Coulomb barrier [33]. The authors observed the suppression of Coulomb-nuclear interference peak, the so-called Coulomb rainbow peak, in the case of the system involving the neutron halo projectile. The same effect was observed but much stronger for the ^{11}Li + ^{208}Pb system [34], involving a two-neutron halo projectile. The reason for this damping of the Coulomb rainbow peak was that the dipole response of these neutron halo projectiles [33,34] is stronger in the system involving the ^{11}Li projectile. Other examples of the reduction of this peak can be found in the literature for collisions involving tightly deformed [35] nuclei, as well as for neutron-halo systems [36–42]. In the case of the system involving strongly deformed target, the Coulomb quadrupole coupling interaction is a long-range potential that acts at long distances, resulting in a reduction of the Fresnel peak. As already mentioned, for the neutron halo systems the long interaction is a result of the dipole term of the Coulomb interaction and the extended matter density, which generate long-range coupling form factors.

A small damping of the Coulomb rainbow peak of the elastic scattering angular distribution was found in the case of reactions induced by the ^{8}B [32] proton halo projectile on the medium mass target ^{58}Ni, as well as on the heavy target ^{208}Pb [43]. As discussed in Ref. [43], the reason for the smaller damping of the Coulomb rainbow peak in the case of reactions induced by this proton halo projectile lies in the fact that its dipole response is lower than in the case of systems involving the neutron halo projectiles mentioned above. However, whether this conclusion is valid for other proton-halo nuclei needs to be further investigated because of the scarce availability of experimental data. Therefore, more experiments need to be performed for ^{17}F on medium-mass targets. This will provide a stronger basis to clearly study the nuclear reaction dynamics induced by exotic nuclei at energies near the Coulomb barrier.

This paper is arranged as follows. In Sec. II, we describe the beam transport and the experimental setup. In Sec. III, we present the data analysis and the experimental results. Sections IV and V are devoted to the comparison of the experimental data with calculations for the quasielastic scattering of ^{17}F on ^{89}Y target performed using the optical model and the CDCC method, respectively. In Sec. VI, the effect of the one-proton stripping reaction on the elastic scattering angular distribution is studied. Finally, in Sec. VI, a summary and some conclusions are presented.

II. EXPERIMENTAL SETUP

This experiment was performed on the radioactive ion beam line in Lanzhou (RIBLL) designed as a double-achromatic antisymmetry separator [44,45], Institute of Modern Physics,
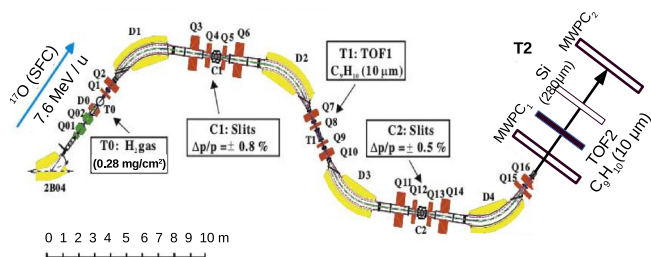
FIG. 1. Schematic view of low-energy radioactive ion beam facility of RIBLL and the experimental setup.

FIG. 3. The plot of energy vs TOF for beam particle identification.

Chinese Academy of Sciences. Figure 1 shows its schematic view. There are three focus points (T0, T1, and T2) under the achromatic mode and two focal planes (C1 and C2) where the horizontal momentum dispersion ($\Delta x/(\Delta p/p)$) is about 20 mm/%. The primary beam $^{17}O^{8+}$ with a beam intensity of 1 pµA was accelerated up to 7.6 MeV/u, passed through 21-µm-thick aluminum foil, and then bombarded a H_2 gas target installed at T0 of RIBLL. The gas is confined into a cylindrical cell with 30-mm-diameter windows and a length of 80 mm. The forward and backward windows were covered by Havar foils 2.5 µm thick. The gas cell was cooled around 5 °C by a water-cooling system and the gas pressure was kept at around 600 Torr. The secondary beam ^{17}F was produced by the $^1H(^{17}O,^{17}F)n$ reaction and then was separated, purified and transported by RIBLL to the secondary target chamber at T2 as shown in Fig. 1. At T1 and T2, two plastic scintillators (C_9H_{10}) 10 µm thick were installed in the beam line to give the time of flight (TOF) information with 1680-cm flight length. The time resolution of TOF is less than 140 ps for 25 MeV/u ^{40}Ar. Each plastic scintillator is connected with an R2083 photomultitube (PMT).

The schematic view of detector setup is shown in Fig. 2. Two multiwire proportional chambers (MWPC) were installed 1666 and 1285 mm in front of the secondary target ^{89}Y. Therefore, the beam position on the secondary target can be determined by analyzing the two-dimensional hit positions measured by two MWPCs. Two collimators with diameter $\phi = 30$ mm were installed behind the two MWPCs and in front of the secondary target to limit the beam spot. The secondary target ^{89}Y with the thickness of 0.981 mg/cm^2 was tilted at 65° with respect to the beam line. Around the ^{89}Y target four sets of ΔE-E detector telescopes were symmetrically mounted along the beam line and cover the angular range of 15−115°. Each
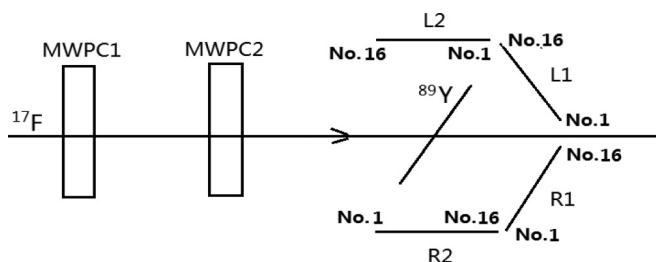

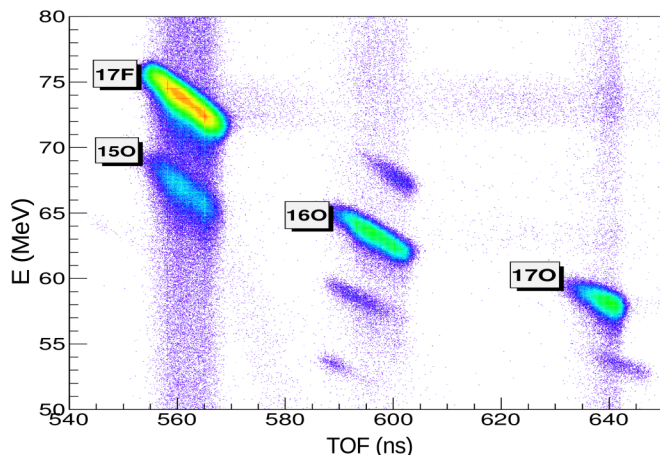FIG. 2. The schematic top view of detector setup of this experiment.

telescope is composed of double-sided silicon strip detectors (DSSD) 65 µm thick and 50 × 50 mm^2 in area and square silicon detectors (SSD) 300 µm thick and 50 × 50 mm^2 in area. The SSD is mounted behind DSSD, which had a strip 3 mm wide and 0.1 mm thick. The distances from the center of DSSD to the target center are 72 and 77 mm, respectively. Behind the ^{89}Y target along the beam line a plastic scintillation detector (not shown in Fig. 2) 5 mm thick and 100 × 100 mm^2 in area was installed to monitor the beam. Its signals were read out by the multipixel photocounter (MPPC). It has been indicated that this detector setup can be used for low-energy RIB study [46].

III. DATA ANALYSIS and RESULTS

The experiment was performed in two phases. The first phase was to identify the secondary beam and the second was to measure the reactions of the secondary beam on the secondary target. At first, a silicon detector 300 µm thick was inserted into the beam line between MWPC2 and the plastic scintillation detector at T2 as an E detector to stop the beam. Figure 3 shows a typical plot of E-TOF for beam particle identification. It is shown that the produced ^{17}F can be clearly separated from ^{16}O and ^{17}O. The purity and the beam intensity of the produced ^{17}F are more than 60% and around 3×10^4 pps, respectively. In Fig. 3, although ^{17}F and ^{15}O have the similar TOF values, ^{15}O cannot give the contaminant for ^{17}F counts due to the significant energy differences between them. It is still possible for ^{17}F to be distinguished from the energy spectrum of DSSDs. The detailed analysis is shown in Refs. [46,47]. Then, the silicon detector was removed from the beam line and only TOF method was used. The energy of the transported ^{17}F at the center of ^{89}Y target is around 59 MeV with the spread ($\sigma = 1.1$ MeV). In order to obtain 50-MeV ^{17}F, a aluminum degrader was inserted in front of the first plastic scintillator at T1, and the energy spread is $\sigma = 1.1$ MeV.

Figure 4 shows two typical energy spectra of ^{17}F on ^{89}Y target collected at the different angles in the frame of laboratory system. Since the energy resolution of the silicon strip detectors was around 1%, the excited state at 495 keV in ^{17}F cannot be separated from the ground state. However, in the calculations
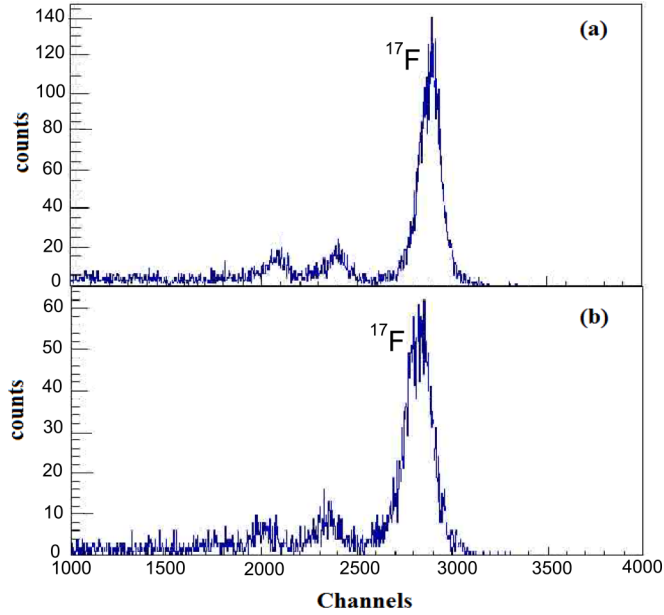
FIG. 4. Typical energy spectra of silicon strip detectors at the different angles in the frame of laboratory system. (a) 76° and (b)109°.

the contribution of the first excited state will be considered (see Sec. V). Since energies of ^{16}O from ^{17}F breakup are close to that of the incident ^{17}F, especially at backward angles. So it is not easy to separate ^{16}O from the scattered ^{17}F in one-dimensional energy spectra. Maybe a small part of ^{16}O is mixed into the event of scattered ^{17}F (see Sec. V).

In the angular distribution of elastic scattering, the differential cross sections are normalized to the differential cross sections of Rutherford scattering, and the ratios are plotted as a function of scattering angles. The Monte Carlo method is applied to simulate the Rutherford scattering with the experimental solid angle. The ratio of reaction differential cross sections to the differential cross sections of Rutherford scattering is obtained by

$$\frac{d\sigma(\theta)}{d\sigma_{Ru}(\theta)} = C \frac{N(\theta)}{N_{Ru}(\theta)}, \qquad (1)$$

where the parameter C is a normalization constant which is determined by assuming that the elastic scattering is a pure Rutherford scattering in a region of small scattering angles (much smaller than the grazing angle). $N(\theta)$ and $N_{Ru}(\theta)$ are the elastic scattering events and Rutherford scattering events with the same solid angle at any scattering angle θ in the frame of laboratory system, respectively.

In this experiment, $N(\theta)$ is the experimental counts of ^{17}F scattering on ^{89}Y target and $N_{Ru}(\theta)$ is obtained from the Monte Carlo simulation. The detailed simulation information is shown in Ref. [46]. The experimental scattering events are normalized to the simulated events at the angle of 22° where the elastic scattering is expected to be a pure Rutherford scattering. The results are displayed in Fig. 5 with filled circles. Here only the statistical error is considered. In comparison with the beam intensity of stable nuclei, that of radioactive ion beam (RIB) is lower by several magnitudes; moreover, the beam spot is
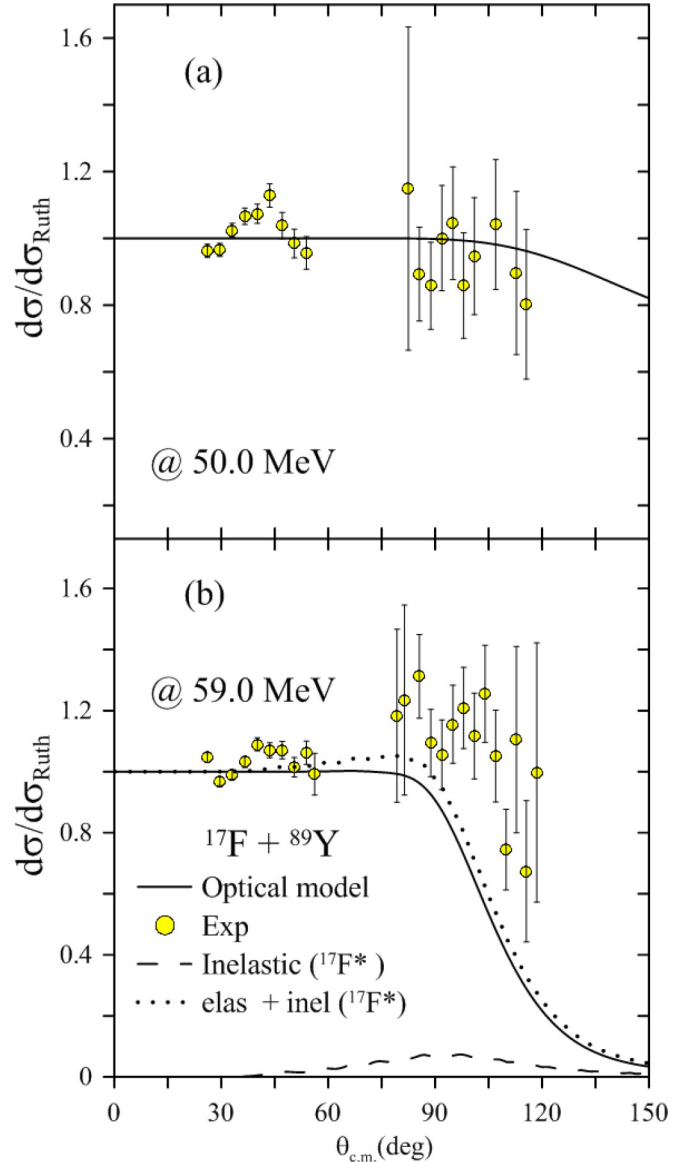

FIG. 5. Differential cross section, relative to Rutherford, for the scattering of ^{17}F on ^{89}Y at (a) $E_{\text{lab}} = 50$ MeV and (b) $E_{\text{lab}} = 59$ MeV. The solid line corresponds to the results of optical model calculations and the circles to the current data. The dashed line represents the results of CC calculations normalized by Rutherford's for the first exited state of ^{17}F projectile. The dotted line stands for the theoretical quasielastic cross section. See text for details.

larger. Therefore, the beam quality is worse. Generally, the experimental data using RIB have large error bars, especially at subbarrier energies, for example, in the experiments of ^{6}He + ^{9}Be [48], ^{6}He + ^{27}Al [49], and ^{8}B + ^{27}Al [50] at the RIBRAS facility, Brazil; ^{8}B + ^{58}Ni [19] at the TwinSol facility at the University of Notre Dame, USA; and ^{11}Li + ^{208}Pb [34] at the ISAC-II line at the TRIUMF facility, Canada. The present data also have the same usual error bars found in measurements mentioned above. Figure 5(a) shows the normalization results of elastic scattering for 50 MeV ^{17}F on ^{89}Y target. Since 50 MeV is far below the Coulomb barrier of the ^{17}F + ^{89}Y

system, the scattering of ^{17}F on ^{89}Y target is almost pure Rutherford scattering. It is observed that the ratios keep the unity at both small and large angles. It indicates that the normalization method is right.

IV. OPTICAL POTENTIAL CALCULATION, COMPARISON WITH DATA, AND DISCUSSION

In this section, we present a comparison of results of optical model calculations with the measured elastic scattering angular distributions. The idea is to perform a one-channel calculation with an optical potential that does not take into account polarizations produced by the strong coupling of the elastic channel and other direct reaction mechanisms. In this way, if the theoretical calculations coincide with the experimental data, one can conclude that there are no important couplings with the elastic channels or there are important couplings but their polarizations are of opposite signs so that their net effect is negligible. On the other hand, if the theoretical angular distribution does not coincide with the data, this means that there are important dynamic or static effects not included in the one-channel calculations that deserves to be studied in details.

In the optical model calculations, the double-folding São Paulo potential [51,52] was used as an optical potential for both real and imaginary parts. This potential has the advantage of having a systematics of the matter densities and no free parameters. It has been extensively used in many theoretical calculations, especially in coupled-channel calculations [1,53,54]. It has been also used for the determination of the energy dependence of the optical potential at near barrier energies for weakly bound nuclei [15,55]. The imaginary part was taken equal to the real part with the strength coefficient of 0.78. This approximation has been proven to be suitable for the description of the elastic cross section of many systems in the energy region where there are no strong couplings expected between the elastic channel and other direct reaction channels [56].

The use of double-folding potentials for both real and imaginary parts in optical model calculations is not a universally accepted procedure. The São Paulo potential was deduced from scattering of stable nuclei, mostly tightly bound and not very light nuclei. Nevertheless, its matter density systematic has been compared with the ones of weakly bound stable nuclei like ^{6,7}Li [57], and it has been shown that the systematics reproduce rather well the matter densities of these nuclei at the surface region (the one that is more relevant for the elastic scattering). It has been also used for describing the total fusion cross section of the ^{8}B + ^{58}Ni system [58]. The systematic value of the matter densities for ^{8}B, a proton halo drip line nucleus, has been compared with microscopic Hartree-Fock Bogolyubov calculations in Ref. [58]. It was shown that both microscopic and systematic matter densities produced very similar total fusion cross section for the ^{8}B + ^{58}Ni system at near-barrier energies [58]. The use of the imaginary part with the same geometry of the real São Paulo potential was proposed for the region of energies where the coupling of the elastic channel and other reaction mechanism is weak [56], as mentioned above. We use the São Paulo potential at near-barrier energies to seek for evidence of important couplings (dynamic effects)

or static effects (like cluster structure) not considered in São Paulo potential systematics.

In Fig. 5, we show the results of our optical model calculations (full line) compared with the experimental data. In Fig. 5(a), the theoretical angular distribution agrees with the experimental data. This agreement emphasizes that the method of the data reduction is correct. From Fig. 5(b), one can see that although the agreement of the optical model results and the data are satisfactory, the theoretical cross sections are smaller than the experimental data in the region near the Coulomb rainbow peak and the angles are larger than that. It is then important to clarify if this disagreement comes from dynamic effects (couplings of the elastic scattering with direct reaction channels, like the breakup, etc) or rather from static effects due to the proton halo structure of the ^{17}F in its first excited state that makes it binding energy as small as 0.6 MeV. For this purpose, we perform continuum discretized coupled-channel calculations as described in the next section.

As already mentioned, the measured angular distribution corresponds to the quasielastic process, that is, the sum of the elastic cross section and the inelastic cross section of the first excited state of the projectile. To elucidate if the difference between the theoretical elastic angular distribution and the experimental data in Fig. 5(b) corresponds to the contribution of the inelastic cross section of the first excited state of the projectile, we performed coupled-channel calculations including only the first excited state of the ^{17}F. In this way, only the ground state of the target and the ground state ($5/2^+$) and the first excited state ($1/2^+$, $\varepsilon = 0.49$ MeV) of the projectile were included on the coupled scheme. To describe the transitions between the projectile states, a model-independent procedure to account for the nuclear and Coulomb deformations was used. The electromagnetic transition $B(E_2)$ was taken from the literature (25.0 in W.u.) [59]. The strength of the Coulomb deformation in this prescription is

$$P_\lambda(k) = \frac{\sqrt{(2I+1)B(E_2)}}{\langle I K \lambda 0 | I' k \rangle}, \qquad (2)$$

where λ is the multipolarity of the transition and I,k are the spin and projection of the states, respectively.

The nuclear deformation is

$$\delta_\lambda(k) = \frac{P_\lambda(k)4\pi}{3ZR}, \qquad (3)$$

where Z is the nuclear charge and $R = r_0(A_p^{1/3} + A_t^{1/3})$, where $r_0 = 1.06$ fm is the reduced radius and A_p, A_t are the mass number of the projectile and target, respectively. For the real part of the optical potential, the São Paulo potential was used. Because some intrinsic nuclear states were taken into account in this CC calculation, to avoid double counting, the strength coefficient of the imaginary part of the optical potential has to be decreased. As the breakup channel is present as one important reaction mechanism for this system, we adopted a strength coefficient of 0.6. It has been shown that this factor accounts for the missing couplings to dissipative processes, as well as for the coupling to continuum states, which are not explicitly considered in the calculations [53,54,60–63].

The results of the CC calculations for the inelastic cross section of the first excited state of the projectile are shown

in Fig. 5(b) by the dashed line. The sum of the elastic plus inelastic divided by Rutherford's cross section is represented by the dotted line in this figure. One can see that although the inelastic cross section is small in the angular range of the measured cross section, it is not completely negligible and its inclusion slightly improves the agreement of the theoretical prediction with the experimental data.

V. CDCC CALCULATION AND COMPARISON WITH EXPERIMENT DATA

In this section, we present the result of CDCC calculation and its comparison with the experimental data. The reaction considered here, $^{17}F + ^{89}Y$, is treated within a three-body model ($p + ^{16}O + ^{89}Y$), which is based on a simple valence proton + core picture of ^{17}F projectile. The ^{17}F states are treated as single-particle configurations of the valence proton coupled to the ground state of ^{16}O. Thus, the ^{17}F ground state $(5/2^+)$ and bound excited state $(1/2^+)$ are described as pure $1d_{5/2}$ and $2s_{1/2}$ configurations, respectively. A Woods-Saxon potential (with central and spin-orbit components) with parameters taken from Ref. [64] is used to produce the ^{17}F wave functions. This potential reproduces the separation energy of the ground state and the bound excited state ($E_x = 0.495$ MeV) as well as the position of the $3/2^+$ resonance at $E_x = 5$ MeV. Continuum states with proton-core angular momentum ℓ up to $6\hbar$ were also included and their eigenfunctions were generated with the same $p + ^{16}O$ potential. For each value of ℓ, the continuum was truncated at a maximum excitation energy and discretized into energy bins, following the standard average method used in CDCC calculations. The maximum excitation energy and the number of bins were increased until the convergence of the calculated observables was achieved. In the present case, the convergence was achieved at the maximum energy of 12 MeV and the total number of bins was 106.

For the CDCC calculations, one needs to specify also the proton-target and ^{16}O + target interaction potentials to generate the so-called coupling potentials [65]. These potentials are typically represented by optical potentials which reproduce the elastic scattering at the appropriate energy per nucleon. For the proton-^{89}Y system, we took the global parameterizations of Koning-Delaroche [66], while for the ^{16}O-^{89}Y system, an optical potential with Wood-Saxon form was used. The parameters of the optical potential were taken as $V = 100$ MeV, $R_v = 8.41$ fm, and $a_v = 0.54$ fm for the depth, radius, and diffuseness of the real part and $W = 50$ MeV, $R_w = 5.85$ fm, and $a_w = 0.65$ fm for its imaginary part, which reproduced the elastic scattering data of $^{16}O + ^{90}Zr$ at 48 MeV [67] in addition to the standard Coulomb potentials. In the case of the proton-^{89}Y system, we also tested the global potential of Becchetti and Greenlees [68] and the results for both elastic and breakup (not shown here) were very similar.

The calculated differential elastic cross sections, relative to the Rutherford cross section, are displayed in Fig. 6. The circles are the current experimental data and the solid line corresponds to the CDCC calculation results, as discussed above. In Fig. 6(a), the calculation results agree with the experimental data at 50 MeV. It shows that CDCC method is right. In Fig. 6(b), the agreement between the experimental
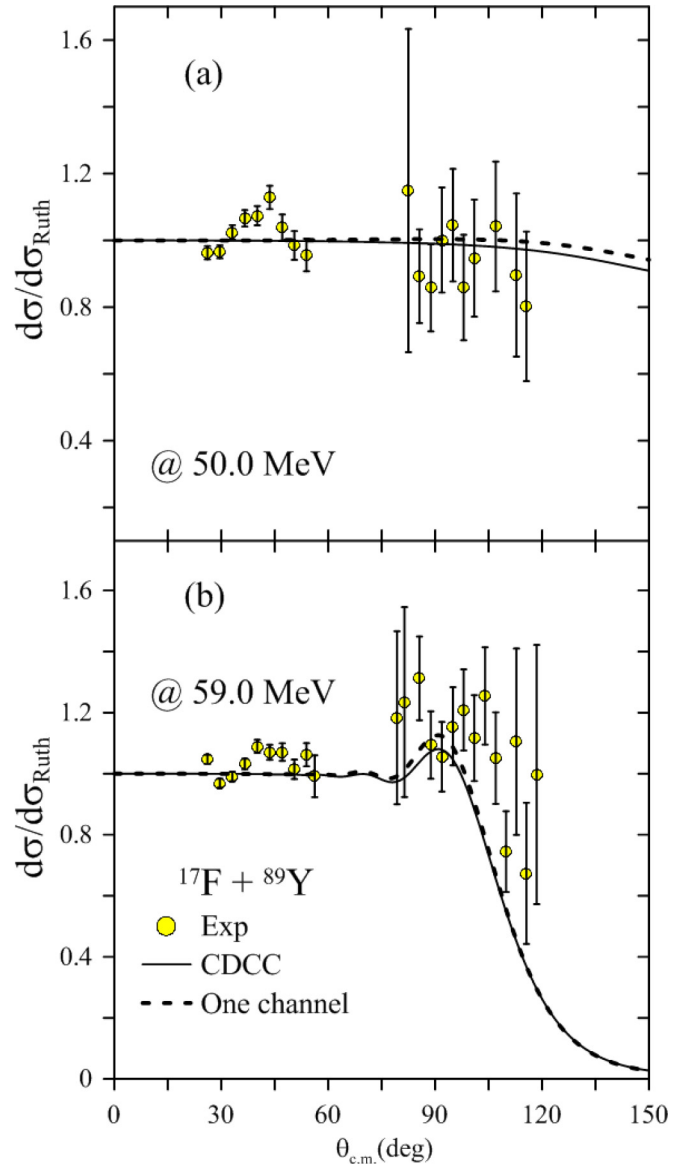

FIG. 6. Differential elastic cross section, relative to Rutherford's, for the scattering of ^{17}F on ^{89}Y at (a) $E_{lab} = 50$ MeV and (b) $E_{lab} = 59$ MeV. The solid line is the CDCC calculation and the circles are the current data.

data at 59 MeV and the theoretical calculation is good at forward angles, whereas they still showed a slight difference at backward angles. First, it is noticeable that the error bars of experimental data at backward angles are bigger than for forward ones, indicating that the accuracy of these data is not as good as those in the forward angles. Second, there are some other contributions from contaminants, such as ^{16}O, which cannot be completely subtracted due to the limitation of the solid detector. Third, as we have discussed above, we should use an optical potential of $^{16}O + ^{89}Y$ at appropriate energy per nucleon. However, there is no such kind of elastic scattering data available in the literature. Instead, we took the potential from a similar system, $^{16}O + ^{90}Zr$, at a lower energy. Since the energy dependence of the optical potential is remarkable
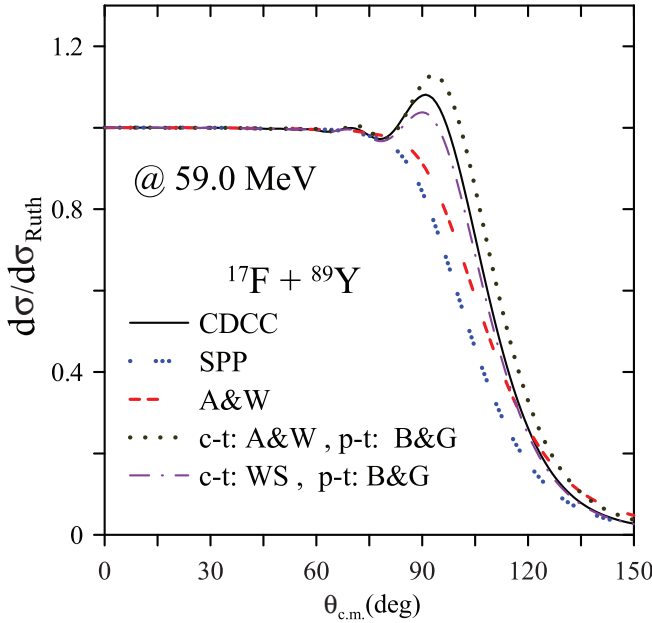
FIG. 7. Derived differential elastic cross section, relative to Rutherford's, for the scattering of ^{17}F on ^{89}Y at $E_{\mathrm{lab}} = 59$ MeV using different proton-target (p-t) and core-target (c-t) optical potentials. For details, see the text.

at energies around the Coulomb barrier, the potential which we used for ^{16}O + ^{89}Y may not be very accurate. In order to clarify this discrepancy, a measurement with more accuracy as well as the experimental data of ^{16}O target at appropriate energy per nucleon is required.

In order to check in detail the sensibility of the derived cross sections to the core-target (c-t) and proton-target (p-t) optical potential used in CDCC calculations, we performed various tests using different optical potentials available in the literature. In Fig. 7, we show the results of these tests. The full line called CDCC corresponds to our previous results shown in Fig. 6(b). The line represented by SPP stands for the results using the double-folding São Paulo potential for both c-t and p-t optical potential with the standard normalizations $N_R = 1.0$ and $N_I = 0.78$ for the real and imaginary parts, respectively. The line represented by A&W stands for the cross section derived using the Akyüz-Winther [69] optical potentials with the same strength for the real and imaginary parts. It is important to notice that these two optical potentials will only describe the elastic scattering in the energy range where no strong couplings with the elastic scattering are expected. This may be the reason why the results using the São Paulo and Akyüz-Winther potentials are quite different from our previous CDCC results. The dot-dashed curve represents the results similar to our previous CDCC results but with changing the p-t potential by the Becchetti and Greenlees potential. Finally, the dotted curve represents the results using the Akyüz-Winther potential for the c-t potential and the Becchetti and Greenlees potential for the p-t interaction. These two last results are quite similar to our previous results, called CDCC in Fig. 7. From these tests, one can see that the results reasonably depend on the c-t optical potential. The calculated angular distributions depend stronger on the p-t optical potential. As expected, the better results are

obtained when global parametrizations derived to describe the elastic scattering angular distributions are used.

In Fig. 6, the results of no continuum couplings are also shown by mean of dashed curves. As a second step, we switch off the first excited state (bound state) of ^{17}F and there was no perceptible difference in the derived elastic scattering angular distribution. Therefore, the inelastic cross section from CDCC calculation is very small when comparing to the elastic channel, in the measured angular interval. For this reason, we remain the same dashed curve, but call it the one-channel calculation in Fig. 6. We emphasize that this one-channel calculation is not the same as in the previous section because here we take into account the cluster configuration of the ^{17}F projectile. One can see that the effect of the coupling to continuum states (both bound-continuum states as well as continuum-continuum state couplings) is not very significant, producing a small hindrance of the Coulomb rainbow peak and a very small enhancement in the case of the reaction at 59 MeV (very hard to see in this linear scale) of the elastic angular distribution at backward angles. A small effect on the elastic scattering angular distribution has also been observed also for ^{8}B proton halo projectile induced reaction on ^{12}C [70], ^{27}Al [50], ^{58}Ni [32], and ^{208}Pb [43], although it has even smaller binding energy of 0.137 MeV and halo structure in its ground state. On the other hand, the reaction induced by neutron halo projectile shows a strong hindrance of the elastic scattering and the cross section normalized by Rutherford's cross section departs from 1.0 for very forward angles, even at energies below the Coulomb barrier [33,34]. As discussed recently in Ref. [43], the main reason for this is the fact that neutron halo systems have strong charge and mass asymmetry between the fragments that they break into. This makes the multipole response of the neutron halo projectiles stronger than the one of the proton halo systems, especially the Coulomb dipole response that is very important for the neutron halo systems [33,34].

VI. EFFECT OF ONE-PROTON STRIPPING ^{89}Y(^{17}F,^{16}O)^{90}Zr REACTION ON THE ELASTIC SCATTERING

In the previous sections, we showed that the elastic scattering angular distributions at 59 MeV could not be properly described by the CDCC calculation. In this section, we will study the effect of one proton stripping reaction ^{89}Y(^{17}F,^{16}O)^{90}Zr on the elastic scattering angular distribution.

The one-proton transfer calculations for the ^{17}F + ^{89}Y reaction were performed using the coupled reaction channels (CRC) method. The São Paulo double-folding potential (V_{SP}) was used for both the real and imaginary parts of the optical potential [$V = (1.0 + N_I)V_{SP}$] with strength coefficient 1.0 for the real part and N_I for the imaginary part. As we are not explicitly considering the coupling to continuum states due to breakup in the CRC calculations, the imaginary part of the optical potential in the entrance partition was multiplied by strength coefficient $N_I = 0.6$ to take into account the contributions of the loss of flux to dissipative channels. On the other hand, in the outgoing partition, the imaginary part of the potential was multiplied by strength coefficient $N_I = 0.78$ because no coupling was explicitly considered. As mentioned
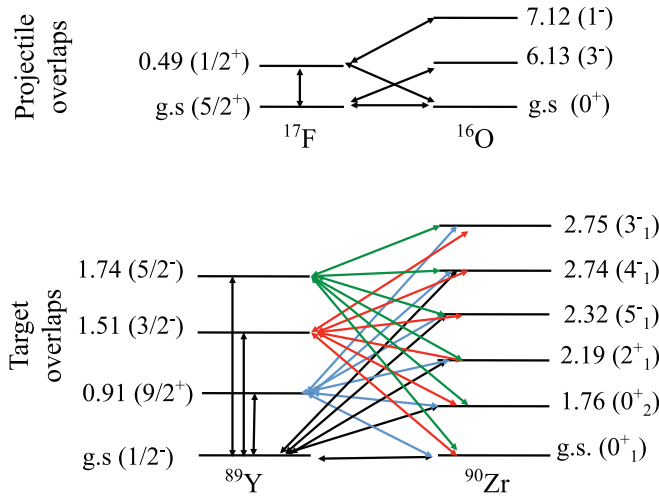
FIG. 8. Coupling scheme considered in the one-proton transfer calculation.

in the previous sections, this procedure has shown to be suitable for describing the elastic scattering cross section for many systems in a wide energy range.

In order to generate the single-particle wave function, Woods-Saxon form factors were used. The reduced radii and diffuseness were set to the standard values of 1.25 and 0.65 fm for both ^{17}F and ^{89}Y nuclei. The depths of the Woods-Saxon potentials were varied in order to fit the experimental one-proton binding energies. The collective states of the projectile and target were taken into account in the CRC calculation. All the states considered in the calculations are shown in the coupling scheme of Fig. 8. The reduced electric transitions probabilities for the collective excitation of the ^{89}Y target and the ^{17}F projectile in the entrance partition were taken from Ref. [59].

It has been shown that the transfer reactions have a strong Q dependence [71,72]. Using semiclassical approximations, Brink *et al.* have shown that the transfer cross section is more probable when the excitation energy for the final states is preferably around E_{opt} which can be obtained by the difference $Q_0 - Q_{\text{opt}}$, where Q_0 is the ground state Q value while the Q_{opt} is defined as

$$Q_{\text{opt}} = E_{c.m.}\left(\frac{Z_p Z_t}{Z_e Z_r} - 1\right). \tag{4}$$

In the expression above, Z_p, Z_t, Z_e, and Z_r are the charges of the projectile, target, ejectile, and residual nuclei, respectively, while $E_{c.m.}$ is the center-of-mass energy.

Notice that when the transferred particle is uncharged, the cross section should achieve the maximum value as $E_{\text{opt}} = Q_0$ because the Q_{opt} is zero and the lower states should be most important to describe the transfer process. However, for the transfer of charged particles, the situation may be completely different because the transfer to excited states of the final nuclei may be more important. In the present case, the $Q_{\text{opt}} = -4.38$ MeV for the one-proton stripping transfer, corresponding to the ^{89}Y(^{17}F,^{16}O)^{90}Zr reaction at 59 MeV of incident energy, which gives $E_{\text{opt}} = 12.1$ MeV.

TABLE I. Spectroscopic amplitudes used in the CRC calculations for one-proton transfer reactions, where j is the spin of the proton orbitals.

Initial State	j	Final State	Spect. ampl.
^{17}F$_{g.s}$(5/2$^+$)	(1$d_{5/2}$)	^{16}O$_{g.s}$(0$^+$)	0.973
^{17}F$_{g.s}$(5/2$^+$)	(1$p_{1/2}$)	^{16}O$_{6.13}$(3$^-$)	0.718
^{17}F$_{0.495}$(1/2$^+$)	(2$s_{1/2}$)	^{16}O$_{g.s}$(0$^+$)	0.975
^{17}F$_{0.495}$(1/2$^+$)	(1$p_{1/2}$)	^{16}O$_{7.12}$(1$^-$)	0.814
^{89}Y$_{g.s}$(1/2$^-$)	(2$p_{1/2}$)	^{90}Zr$_{g.s}$(0$^+$)	1.151
^{89}Y$_{g.s}$(1/2$^-$)	(2$p_{1/2}$)	^{90}Zr$_{1.76}$(0$^+$)	−0.710
^{89}Y$_{g.s}$(1/2$^-$)	(2$p_{3/2}$)	^{90}Zr$_{2.19}$(2$^+$)	0.034
	(1$f_{5/2}$)		−0.107
^{89}Y$_{g.s}$(1/2$^-$)	(1$g_{9/2}$)	^{90}Zr$_{2.32}$(5$^-$)	0.969
^{89}Y$_{g.s}$(1/2$^-$)	(1$g_{9/2}$)	^{90}Zr$_{2.74}$(4$^-$)	0.961
^{89}Y$_{0.909}$(9/2$^+$)	(1$g_{9/2}$)	^{90}Zr$_{g.s}$(0$^+$)	1.000
^{89}Y$_{0.909}$(9/2$^+$)	(1$g_{9/2}$)	^{90}Zr$_{1.76}$(0$^+$)	1.129
^{89}Y$_{0.909}$(9/2$^+$)	(1$g_{9/2}$)	^{90}Zr$_{2.19}$(2$^+$)	1.362
	(2$p_{1/2}$)		0.866
^{89}Y$_{0.909}$(9/2$^+$)	(2$p_{3/2}$)	^{90}Zr$_{2.32}$(5$^-$)	0.042
	(1$f_{5/2}$)		−0.043
	(2$p_{1/2}$)		−0.871
^{89}Y$_{0.909}$(9/2$^+$)	(2$p_{3/2}$)	^{90}Zr$_{2.74}$(4$^-$)	0.060
	(1$f_{5/2}$)		0.019
^{89}Y$_{0.909}$(9/2$^+$)	(2$p_{3/2}$)	^{90}Zr$_{2.75}$(3$^-$)	0.359
	(1$f_{5/2}$)		−0.057
^{89}Y$_{1.507}$(3/2$^+$)	(2$p_{3/2}$)	^{90}Zr$_{g.s}$(0$^+$)	−1.841
^{89}Y$_{1.507}$(3/2$^+$)	(2$p_{3/2}$)	^{90}Zr$_{1.76}$(0$^+$)	0.219
	(2$p_{1/2}$)		−0.011
^{89}Y$_{1.507}$(3/2$^+$)	(2$p_{3/2}$)	^{90}Zr$_{2.19}$(2$^+$)	−0.012
	(1$f_{5/2}$)		0.074
^{89}Y$_{1.507}$(3/2$^+$)	(1$g_{9/2}$)	^{90}Zr$_{2.32}$(5$^-$)	0.042
^{89}Y$_{1.507}$(3/2$^+$)	(1$g_{9/2}$)	^{90}Zr$_{2.74}$(4$^-$)	−0.095
^{89}Y$_{1.507}$(3/2$^+$)	(1$g_{9/2}$)	^{90}Zr$_{2.75}$(3$^-$)	0.940
^{89}Y$_{1.745}$(5/2$^+$)	(1$f_{5/2}$)	^{90}Zr$_{g.s}$(0$^+$)	−2.317
^{89}Y$_{1.745}$(5/2$^+$)	(1$f_{5/2}$)	^{90}Zr$_{1.76}$(0$^+$)	0.031
	(2$p_{1/2}$)		−0.063
^{89}Y$_{1.745}$(5/2$^+$)	(2$p_{3/2}$)	^{90}Zr$_{2.19}$(2$^+$)	−0.136
	(1$f_{5/2}$)		0.181
^{89}Y$_{1.745}$(5/2$^+$)	(1$g_{9/2}$)	^{90}Zr$_{2.32}$(5$^-$)	−0.046
^{89}Y$_{1.745}$(5/2$^+$)	(1$g_{9/2}$)	^{90}Zr$_{2.74}$(4$^-$)	−0.001
^{89}Y$_{1.745}$(5/2$^+$)	(1$g_{9/2}$)	^{90}Zr$_{2.75}$(3$^-$)	−0.057

To perform the CRC calculation in a microscopic way, it is necessary to calculate the spectroscopic amplitudes concerning the projectile and target overlaps. They were obtained from a shell-model calculation by the NUSHELLX code [73]. To obtain the one-proton spectroscopic information related to the projectile overlaps, the structure model Zuker-Buck-McGrory (ZBM) and effective phenomenological ZBM [74] interaction were considered. In this model space, the ^{12}C nucleus is considered as closed core and the 1$p_{1/2}$, 1$d_{5/2}$, and 2$s_{1/2}$ orbitals are taken as the valence space for both protons and neutrons. For the target overlaps, the structure model jj44 and effective interaction jun45 [75] were considered. In this model space, the ^{40}Ca nucleus is considered as closed core and the 1$f_{5/2}$, 2$p_{3/2}$, 2$p_{1/2}$, and 1$g_{9/2}$ orbitals are taken as valence space for protons and neutrons. The spectroscopic amplitudes for the projectile and the target overlaps are shown in Table I.
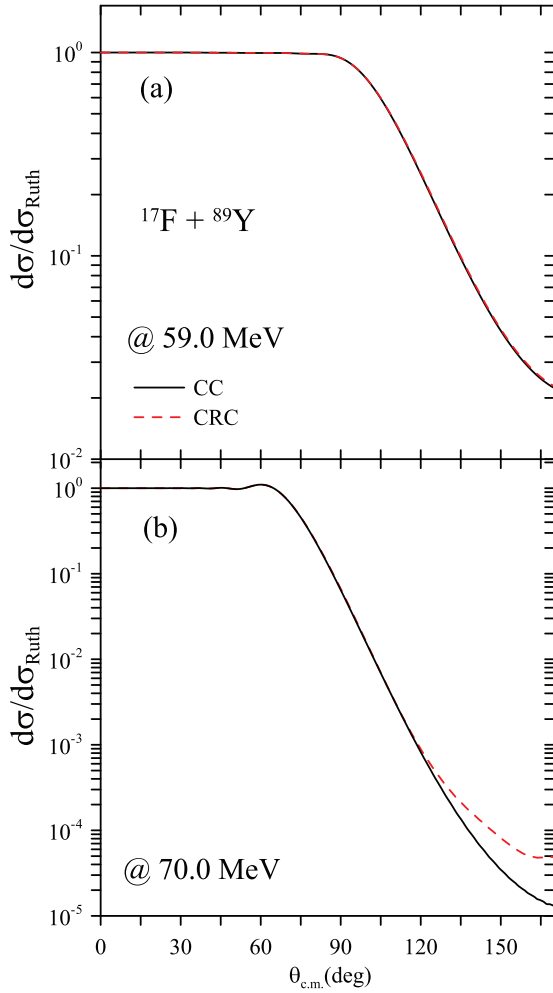
FIG. 9. Comparison of CRC and CC results for the elastic scattering angular distributions for $E_{\text{lab}}(^{17}\text{F}) = 59$ MeV (a) and $E_{\text{lab}}(^{17}\text{F}) = 70$ MeV (b).

The results of the CRC calculations for the elastic scattering angular distributions for $E_{\text{lab}}(^{17}\text{F}) = 59$ MeV are compared with the CC calculations (in which the one-proton transfer channel was switched off) in Fig. 9(a). One can see that the effect of the one-proton transfer channel at $E_{\text{lab}}(^{17}\text{F}) = 59$ MeV on the elastic cross section is negligible. So, this indeed is not the reason for the small disagreement between the CDCC results for the elastic scattering angular distribution and the experimental data observed in Fig. 6 of the previous section.

One can infer that the effect of the one-proton stripping channel on the elastic scattering angular distribution is weak because the incident energy is not high enough to open that channel with high probability. In order to verify this statement, the incident energy of the ^{17}F projectile was increased by 11 MeV and a larger effect on the elastic scattering angular distribution was obtained, as can be seen from Fig. 9(b). Despite the increment of the incident energy, the optimum Q value has no significant change ($Q_{\text{opt}} = -5.12$ MeV) which gives an $E_{\text{opt}} = 12.87$ MeV. So, it would be interesting to measure elastic scattering angular distributions and transfer cross section at higher energies to support our theoretical predictions.

VII. SUMMARY AND CONCLUSIONS

The experiments with 50 and 59 MeV ^{17}F radioactive ion beam impinging on a ^{89}Y target were performed at RIBLL. The elastic scattering angular distributions were measured by using a silicon detector telescope array which covered the range from $15°$ to $115°$ in the laboratory system. The normalization results of 50-MeV $^{17}\text{F} + ^{89}\text{Y}$ keep unity at both small and, within the statistical errors, large angles. The optical model was used to analyze the experimental data of elastic scattering angular distributions.

The double-folding São Paulo potential was used as an optical potential for both real and imaginary parts. For 50 MeV, the results of optical model agree with the experimental data. For 59 MeV, the agreement of the optical model results and the experimental data is quite remarkable. The theoretical cross sections are smaller than the experimental data in the region near the Coulomb rainbow peak. In order to clarify if this disagreement comes from the dynamic effects such as the breakup or rather from static effects due to the proton halo structure of ^{17}F in its first excited state, CDCC calculations were performed. For 50 MeV, the calculation results agree with the experimental data. It indicates that the method of data analysis and CDCC calculation are correct. For 59 MeV, the agreement between the experimental data and the theoretical results is good at forward angles. However, a slight difference is present at backward angles. In order to clarify this discrepancy, a measurement with better statistical accuracy as well as experimental data for the system ^{16}O target at appropriate energy per nucleon is required. It is also found that for proton halo nuclei, the effect of the coupling to the continuum states is not very significant (especially in the case of the reaction induced for the ^{17}F projectile discussed here), only producing a small hindrance of the Coulomb rainbow peak and a very small enhancement of the elastic scattering angular distribution at backward angles. However, the neutron halo projectiles show a strong hindrance of the elastic scattering. The main reason is that the multipole response of neutron halo projectiles, especially Coulomb dipole response, is stronger than that of proton halo systems. More experimental data with higher resolution are needed to further clarify this viewpoint. We would like to emphasize that although the error bars of the experimental data are large, the comparison of the data and the theoretical calculation allows us to conclude that the reactions induced by ^{17}F behave similar to the ones induced by ^{8}B and are different from the ones induced by neutron-halo projectiles.

It was also shown that the one-proton stripping reaction does not affect the elastic scattering angular distribution at the measured energies around the Coulomb barrier. Some indications were found that at higher energies the one-proton transfer reaction may affect the elastic scattering angular distributions at backward angles.

[1] L. F. Canto, P. R. S. Gomes, R. Donangelo, J. Lubian, and M. S. Hussein, Phys. Rep. **596**, 1 (2015).

[2] N. Keeley, R. Raabe, N. Alamanos, and J. L. Sida, Prog. Part. Nucl. Phys. **59**, 579 (2007).

[3] N. Keeley, N. Alamanos, K. W. Kemper, and K. Rusek, Prog. Part. Nucl. Phys. **63**, 396 (2009).

[4] B. B. Back, H. Esbensen, C. L. Jiang, and K. E. Rehm, Rev. Mod. Phys. **86**, 317 (2014).

[5] P. R. S. Gomes, J. Lubian, L. F. Canto, D. R. Otomar, D. R. Mendes, Jr., P. N. de Faria, R. Linares, L. Sigaud, J. Rangel, J. L. Ferreira *et al.*, Few-Body Systems **57**, 165 (2016).

[6] J. J. Kolata, V. Guimarães, and E. F. Aguilera, Eur. Phys. J. A **52**, 1 (2016).

[7] E. F. Aguilera, J. J. Kolata, F. M. Nunes, F. D. Becchetti, P. A. DeYoung, M. Goupell, V. Guimaraes, B. Hughey, M. Y. Lee, D. Lizcano *et al.*, Phys. Rev. Lett. **84**, 5058 (2000).

[8] E. F. Aguilera, J. J. Kolata, F. D. Becchetti, P. A. DeYoung, J. D. Hinnefeld, A. Horvath, L. O. Lamm, H. Y. Lee, D. Lizcano, E. Martinez-Quiroz *et al.*, Phys. Rev. C **63**, 061603(R) (2001).

[9] E. F. Aguilera, P. Amador-Valenzuela, E. Martinez-Quiroz, D. Lizcano, P. Rosales, H. Garcia-Martinez, A. Gomez-Camacho, J. J. Kolata, A. Roberts, L. O. Lamm *et al.*, Phys. Rev. Lett. **107**, 092701 (2011).

[10] K. E. Rehm, H. Esbensen, C. L. Jiang, B. B. Back, F. Borasi, B. Harss, R. V. F. Janssens, V. Nanal, J. Nolen, R. C. Pardo *et al.*, Phys. Rev. Lett. **81**, 3341 (1998).

[11] R. Raabe, J. L. Sida, J. L. Charvet, N. Alamanos, C. Angulo, J. M. Casandjian, S. Courtin, A. Drouart, D. J. C. Durand, P. Figuera *et al.*, Nature (London) **431**, 823 (2004).

[12] J. J. Kolata, V. Guimaraes, D. Peterson, P. Santi, R. White-Stevens, P. A. DeYoung, G. F. Peaslee, B. Hughey, B. Atalla, M. Kern *et al.*, Phys. Rev. Lett. **81**, 4580 (1998).

[13] G. R. Satchler, Phys. Rep. **199**, 147 (1991).

[14] G. R. Satchler and W. Love, Phys. Rep. **55**, 183 (1979).

[15] M. S. Hussein, P. R. S. Gomes, J. Lubian, and L. C. Chamon, Phys. Rev. C **73**, 044610 (2006).

[16] P. R. S. Gomes, J. Lubian, I. Padron, and R. M. Anjos, Phys. Rev. C **71**, 017601 (2005).

[17] J. M. B. Shorto, P. R. S. Gomes, J. Lubian, L. F. Canto, S. Mukherjee, and L. C. Chamond, Phys. Lett. B **678**, 77 (2009).

[18] J. C. Zamora, V. Guimaraes, A. Barioni, A. Lepine-Szily, R. Lichtenthaler, P. N. de Faria, D. R. Mendes, L. R. Gasques, J. M. B. Shorto, V. Scarduelli *et al.*, Phys. Rev. C **84**, 034611 (2011).

[19] E. F. Aguilera, E. Martinez-Quiroz, D. Lizcano, A. Gomez-Camacho, J. J. Kolata, L. O. Lamm, V. Guimaraes, R. Lichtenthaler, O. Camargo, F. D. Becchetti *et al.*, Phys. Rev. C **79**, 021601(R) (2009).

[20] R. Morlock, R. Kunz, A. Mayer, M. Jaeger, A. Muller, J. W. Hammer, P. Mohr, H. Oberhummer, G. Staudt, and V. Kolle, Phys. Rev. Lett. **79**, 3837 (1997).

[21] M. J. G. Borge, J. Deding, P. G. Hansen, B. Jonson, G. Martínez Pinedo, P. Møller, G. Nyman, A. Poves, A. Ritcher, K. Riisager, and O. Tengblad, Phys. Lett. B **317**, 25 (1993).

[22] J. F. Liang, J. R. Beene, H. Esbensen, A. Galindo-Uribarri, J. Gomez del Campo, C. J. Gross, M. L. Halbert, P. E. Mueller, D. Shapira, D. W. Stracener, and R. L. Varner, Phys. Lett. B **491**, 23 (2000).

[23] A. Ozawa, T. Suzuki, and I. Tanihata, Nucl. Phys. A **693**, 32 (2001).

[24] H. Kitagawa, N. Tajima, and H. Sagawa, Z. Phys. A **358**, 381 (1997).

[25] J. F. Liang, J. R. Beene, H. Esbensen, A. Galindo-Uribarri, J. Gomez del Campo, C. J. Gross, M. L. Halbert, P. E. Mueller, D. Shapira, D. W. Stracener *et al.*, Phys. Rev. C **65**, 051603 (2002).

[26] J. Liang, J. R. Beene, A. Galindo-Uribarri, J. Gomez del Campo, C. J. Gross, P. A. Hausladen, P. E. Mueller, D. Shapira, D. W. Stracener, R. L. Varner *et al.*, Phys. Rev. C **67**, 044603 (2003).

[27] M. Romoli, E. Vardaci, M. Di Pietro, A. De Francesco, A. De Rosa, G. Inglima, M. La Commara, B. Martin, D. Pierroutsakou, M. Sandoli *et al.*, Phys. Rev. C **69**, 064614 (2004).

[28] J. C. Blackmon, F. Carstoiu, L. Trache, D. W. Bardayan, C. R. Brune, C. A. Gagliardi, U. Greife, C. J. Gross, C. C. Jewett, R. L. Kozub *et al.*, Phys. Rev. C **72**, 034606 (2005).

[29] G. L. Zhang, C. L. Zhang, H. Q. Zhang, C. J. Lin, D. Y. Pang, X. K. Wu, H. M. Jia, G. P. An, Z. D. Wu, X. X. Xu *et al.*, Eur. Phys. J. A **48**, 65 (2012).

[30] M. Mazzocco, C. Signorini, D. Pierroutsakou, T. Glodariu, A. Boiano, C. Boiano, F. Farinon, P. Figuera, D. Filipescu, L. Fortunato *et al.*, Phys. Rev. C **82**, 054604 (2010).

[31] F. M. Nunes and I. J. Thompson, Phys. Rev. C **59**, 2652 (1999).

[32] J. Lubian, T. Correa, E. F. Aguilera, L. F. Canto, A. Gomez-Camacho, E. M. Quiroz, and P. R. S. Gomes, Phys. Rev. C **79**, 064605 (2009).

[33] A. DiPietro, G. Randisi, V. Scuderi, L. Acosta, F. Amorini, M. J. G. Borge, P. Figuera, M. Fisichella, L. M. Fraile, J. Gomez-Camacho *et al.*, Phys. Rev. Lett. **105**, 022701 (2010).

[34] M. Cubero, J. P. Fernandez-Garcia, M. Rodriguez-Gallardo, L. Acosta, M. Alcorta, M. A. G. Alvarez, M. J. G. Borge, L. Buchmann, C. A. Diget, H. A. Falou *et al.*, Phys. Rev. Lett. **109**, 262701 (2012).

[35] C. E. Thorn, M. J. LeVine, J. J. Kolata, C. Flaum, P. D. Bond, and J. C. Sens, Phys. Rev. Lett. **38**, 384 (1977).

[36] A. Di Pietro, V. Scuderi, A. M. Moro, L. Acosta, F. Amorini, M. J. G. Borge, P. Figuera, M. Fisichella, L. M. Fraile, J. Gomez-Camacho *et al.*, Phys. Rev. C **85**, 054607 (2012).

[37] M. Mazzocco, C. Signorini, M. Romoli, A. De Franesco, M. Di Pietro, E. Vardaci, K. Yoshida, R. Yoshida, A. Bonetti, A. De Rosa, T. Glodariu *et al.*, Eur. Phys. J. A **28**, 295 (2006).

[38] V. Morcelle, K. C. C. Pires, M. Rodríguez-Gallardo, R. Lichtenthaler, A. Lépine-Szily, V. Guimarães, P. N. de Faria, D. R. Mendes, Jr., A. M. Moro, L. R. Gasques *et al.*, Phys. Lett. B **732**, 228 (2014).

[39] A. M. Sánchez-Benítez, D. Escrig, M. A. G. Álvarez, M. V. Andrés, C. Angulo, M. J. G. Borge, J. Cabrera, S. Cherubini, P. Demarelt, J. M. Espino *et al.*, Nucl. Phys. A **803**, 30 (2008).

[40] O. R. Kakuee, J. Rahighi, A. M. Sanchez-Benitez, M. V. Andreś, S. Cherubini, T. Davinson, W. Galster, J. Gomez-Camacho, A. M. Laird, M. Lamehi-Rachti *et al.*, Nucl. Phys. A **728**, 339 (2003).

[41] L. Acosta, A. M. Sánchez-Benítez, M. E. Gómez, I. Martel, F. Pérez-Bernal, F. Pizarro, J. Rodríguez-Quintero, K. Rusek, M. A. G. Alvarez, M. V. Andrés *et al.*, Phys. Rev. C **84**, 044604 (2011).

[42] L. Standylo, L. Acosta, C. Angulo, R. Berjillos, J. A. Duenas, M. S. Golovkov, N. Keeley, T. Keutgen, I. Martel, M. Mazzocco *et al.*, Phys. Rev. C **87**, 064603 (2013).

[43] J. Rangel, J. Lubian, L. F. Canto, and P. R. S. Gomes, Phys. Rev. C **93**, 054610 (2016).

[44] J. W. Xia, W. L. Zhan, B. W. Wei, Y. J. Yuan, M. T. Song, W. Z. Zhang, X. D. Yang, P. Yuan, D. Q. Gao, H. W. Zhao *et al.*, Nucl. Instr. Method Phys. Res. A **488**, 11 (2002).

[45] J. J. He, S. W. Xu, P. Ma, J. S. Wang, Y. Y. Yang, J. B. Ma, L. Y. Zhang, L. Li, X. Q. Yu, S. L. Jin *et al.*, Nucl. Instrum. Meth. Phys. Res. A **680**, 43 (2012).

[46] G. X. Zhang, G. L. Zhang, C. J. Lin, W. W. Qu, L. Yang, N. R. Ma, L. Zheng, H. M. Jia, L. J. Sun, X. X. Liu *et al.*, Nucl. Instrum. Meth. Phys. Res. A **846**, 23 (2017).

[47] G.-L. Zhang, Y.-J. Yao, G.-X. Zhang, Z.-W. Jiao, C.-J. Lin, Y.-Z. Niu, W.-W. Qu, L. Yang, N.-R. Ma, and L. Zheng *et al.*, Nucl. Sci. Tech. **28**, 104 (2017).

[48] K. C. C. Pires, R. Lichtenthaler, A. Lepine-Szily, V. Guimaraes, P. N. de Faria, A. Barioni, D. R. Mendes, Jr., V. Morcelle, R. P. Condori, M. C. Morais *et al.*, Phys. Rev. C **83**, 064603 (2011).

[49] E. A. Benjamim, A. Lépine-Szily, D. R. Mendes Junior, R. Lichtenthäler, V. Guimarães, P. R. S. Gomes, L. C. Chamon, M. S. Hussein, A. M. Moro, A. Arazi *et al.*, Phys. Lett. B **647**, 30 (2007).

[50] V. Morcelle, R. Lichtenthaler, A. Lepine-Szily, V. Guimaraes, K. C. C. Pires, J. Lubian, D. R. Mendes, Jr., P. N. de Faria, J. J. Kolata, F. D. Becchetti *et al.*, Phys. Rev. C **95**, 014615 (2017).

[51] L. C. Chamon, D. Pereira, M. S. Hussein, M. A. C. Ribeiro, and D. Galetti, Phys. Rev. Lett. **79**, 5218 (1997).

[52] L. C. Chamon, B. V. Carlson, L. R. Gasques, D. Pereira, C. De Conti, M. A. G. Alvarez, M. S. Hussein, M. A. C. Ribeiro, E. S. Rossi, and C. P. Silva, Phys. Rev. C **66**, 014610 (2002).

[53] M. J. Ermamatov, F. Cappuzzello, J. Lubian, M. Cubero, C. Agodi, D. Carbone, M. Cavallaro, J. L. Ferreira, A. Foti, V. N. Garcia *et al.*, Phys. Rev. C **94**, 024610 (2016).

[54] M. Cavallaro, F. Cappuzzello, M. Bondi, D. Carbone, V. N. Garcia, A. Gargano, S. M. Lenzi, J. Lubian, C. Agodi, F. Azaiez *et al.*, Phys. Rev. C **88**, 054601 (2013).

[55] P. R. S. Gomes, I. Padron, J. O. Fernández Niello, G. V. Martí, M. D. Rodríguez, O. A. Capurro, A. J. Pacheco, J. E. Testoni, A. Arazi, and J. Lubian *et al.*, J. Phys. G **31**, S1669 (2005).

[56] L. Gasques, L. Chamon, P. R. S. Gomes, and J. Lubian, Nucl. Phys. A **764**, 135 (2006).

[57] D. P. Sousa, D. Pereira, J. Lubian, L. C. Chamon, J. R. B. Oliveira, E. S. Rossi, Jr., C. P. Silva, P. N. de Faria, R. Lichtenthaler, and M. A. G. Alvarez, Nucl. Phys. A **836**, 1 (2010).

[58] J. Rangel, J. Lubian, P. R. S. Gomes, B. V. Carlson, L. C. Chamon, A. G. Camacho, Eur. Phys. J. A **49**, 57 (2013).

[59] National Nuclear Data Center, www.nndc.bnl.gov.

[60] D. Pereira, J. Lubian, J. Oliveira, D. Sousa, and L. Chamon, Phys. Lett. B **670**, 330 (2009).

[61] F. Cappuzzello, D. Carbone, M. Cavallaro, M. Bond, C. Agodi, F. Azaiez, A. Bonaccorso, A. Cunsolo, L. Fortunato, A. Foti *et al.*, Nat. Commun. **6**, 6743 (2015).

[62] D. Carbone, J. Ferreira, F. Cappuzzello, J. Lubian, C. Agodi, M. Cavallaro, A. Foti, A. Gargano, S. Lenzi, R. Linares *et al.*, Phys. Rev. C **95**, 034603 (2017).

[63] M. J. Ermamatov, R. Linares, J. Lubian, J. L. Ferreira, F. Cappuzzello, D. Carbone, M. Cavallaro, M. Cubero, P. N. de Faria, A. Foti, G. Santagati, and V. A. B. Zagatto, Phys. Rev. C **96**, 044603 (2017).

[64] J. M. Sparenberg, D. Baye, and B. Imanishi, Phys. Rev. C **61**, 054610 (2000).

[65] N. Austern, Y. Iseri, M. Kamimura, M. Kawai, G. Rawitscher, and M. Yahiro, Phys. Rep. **154**, 125 (1987).

[66] A. Koning and J. Delaroche, Nucl. Phys. A **713**, 231 (2003).

[67] M. Alvarez, L. Chamon, D. Pereira, E. Rossi, C. Silva, L. Gasques, H. Dias, and M. Roos, Nucl. Phys. A **656**, 187 (1999).

[68] F. D. Becchetti and G. W. Greenlees, Phys. Rev. **182**, 1190 (1969).

[69] R. A. Broglia and A. Winther, *Heavy Ion Reactions* (Westview Press, Boulder, CO, 2004).

[70] B. Paes, J. Lubian, P. R. S. Gomes, and V. Guimaraes, Nucl. Phys. A **890-891**, 1 (2012).

[71] P. J. A. Buttle and L. J. B. Goldfarb, Nucl. Phys. A **176**, 299 (1971).

[72] D. M. Brink, Pyhs. Lett. B **40**, 37 (1972).

[73] NUSHELLX for Windows and Linux, http://www.garsington.eclipse.co.uk/.

[74] A. P. Zuker, B. Buck, and J. B. McGrory, Phys. Rev. Lett. **21**, 39 (1968).

[75] M. Honma, T. Otsuka, T. Mizusaki, and M. Hjorth-Jensen, Phys Rev C **80**, 064323 (2009).